Proceedings of the 21st ICSMGE, Vienna, Austria, 14 – 19 June 2026. Pistrol, Adam & Schweiger (eds.)
Published by: ÖGG, Austrian Society for Geomechanics, Salzburg, Austria, ISBN 978-3-9503898-4-5
https://doi.org/10.53243/ICSMGE2026-804

Numerical investigations of the environmental impact of continuous caisson group penetration in undrained clay

Xiaoxiang Wang, Maosong Huang, Jian Yu
Key Laboratory of Geotechnical and Underground Engineering of Ministry of Education, Tongji University, Shanghai, China
Department of Geotechnical Engineering, Tongji University, Shanghai, China, 002yujian@tongji.edu.cn

Zhongjie Zhang, Haoran Wang
Shanghai Urban Construction Design & Research Institute (Group) Co., Ltd., Shanghai, China

ABSTRACT: The continuous caisson group method provides a novel prefabricated construction approach for large-scale underground structures. Accurately predicting the deformation evolution of surrounding soil during continuous caisson penetration is crucial for ensuring the safety of both caisson structures and adjacent environments. This study establishes a 3D finite element model of continuous caisson group penetration based on an actual underground station project, investigating environmental impact mechanism during sequential twin-caisson installation. Validated against empirical formulas, the model evaluates synchronous and asynchronous installation schemes. Results reveal mutual attraction effect between caissons under both schemes, demonstrating that soil deformation patterns around twin caissons result from nonlinear superposition of single-caisson responses. Comparative analysis confirms synchronous installation minimizes surface settlement and structural response, establishing it as the optimal solution for twin-caisson installations. Parametric studies within this optimal scheme quantify key construction factors: (a) Increased horizontal spacing progressively diminishes inter-caisson interaction to negligible level, with soil deformation and structural response converging toward single-caisson penetration behavior; (b) Elevated soil-caisson interface friction heightens soil sensitivity, triggering nonlinear growth in soil deformation and structural displacement - an effect exacerbated at greater penetration depths. These findings elucidate environmental impact mechanism of continuous caisson group penetration, providing scientific basis for minimizing environmental impact in congested urban areas through optimized installation sequences and parameter control.

KEYWORDS: Continuous caisson group, 3D finite element model, mutual attraction effect, environmental impact.

1 INTRODUCTION

Urban densification and the imperative for sustainable infrastructure development are driving unprecedented expansion in underground space utilization. Compared to cut-and-cover methods, the continuous caisson group construction technique offers distinct advantages for creating large-scale underground structures (Zhao & Zhou 2013). This approach involves sinking prefabricated segments in batches to designated positions, subsequently interconnecting them to form integrated underground spaces. Its superior performance in construction quality, efficiency, and environmental sustainability establishes an industrialized, prefabricated green construction paradigm for underground development in densely urbanized centers. Nevertheless, the sequential installation of multiple adjacent caissons - forming a "continuous caisson group" - introduces unique geotechnical challenges. The cumulative and interactive ground movements induced during each caisson's progressive penetration pose significant risks to nearby structures, utilities, and services, particularly in built-up urban environments with extremely low tolerance for ground deformation.

Previous research has primarily focused on ground displacements induced by single-caisson installations and their impacts on adjacent infrastructure (e.g., buried pipelines, tunnels, and buildings). Although twin-caisson construction has been widely implemented globally, the complex interaction effects and cumulative impacts arising from sequential installations remain inadequately understood (Newman & Wong 2011). New & Bowers (1994) proposed a methodology correlating caisson shaft depth with surface settlement in greenfield conditions, widely adopted during preliminary design stages. Subsequently, New (2017) collated field data from 13 circular caisson projects, introducing a novel variable governing the decay-to-zero of surface settlement at radial distances from the shaft. Le et al. (2019) empirically developed a predictive framework for surface displacement by synthesizing centrifuge tests and field data. However, surface displacement profiles derived from these methods represent mere linear superposition of individual deformation curves, neglecting potential interaction effects between multiple caissons. Compounding this issue, studies have confirmed that the superposition of displacement fields from adjacent installations is fundamentally nonlinear, being critically influenced by installation sequence, soil-structure interaction, and evolving stress states within the soil mass (Zhang et al. 2019; Lai et al. 2021; Yu et al. 2022; Huang et al. 2023). Consequently, predicting and mitigating environmental impacts of continuous caisson groups requires fundamental understanding of how installation sequences govern the spatiotemporal evolution of soil displacement and stress redistribution.

To address these gaps, this study employs three-dimensional numerical modeling to unravel the fundamental mechanisms controlling the environmental impact of twin caissons installations. This study innovatively proposes the existence of "mutual attraction effect" during caissons group penetration, a phenomenon systematically investigated through comparative analysis of synchronous and asynchronous installation schemes. The numerical model, validated against empirical formulas, enables the identification of the optimal installation sequence for twin caissons. Beyond sequence optimization, parametric studies examine key controlling parameters-including penetration depth, horizontal caisson spacing, and soil-caisson interface friction coefficient-to evaluate their influence on surface displacement, structural response, and the mutual attraction effect itself. Through this comprehensive approach, the study elucidates the causes and environmental implications of inter-caisson interactions, providing engineers with scientific basis for selecting appropriate installation sequences and critical design parameters, ultimately enabling safer, more efficient, and less disruptive underground construction in sensitive urban environments.

2 ENGINEERING BACKGROUND

As illustrated in Figure 1, the caisson group project pertains to an underground station. The main structure has a total length of 283.4 m and is longitudinally divided into seven caissons. The two end sections comprise Caisson 1# and Caisson 7#, each measuring 33.1 m in length, 23.4 m in width, and 27 m in depth. The five standard sections (Caissons 2# to 6#) each measure 44.42 m in length, 25.5 m in width, and 25 m in depth. The longitudinal clear spacing between adjacent caissons is 2.5 m.

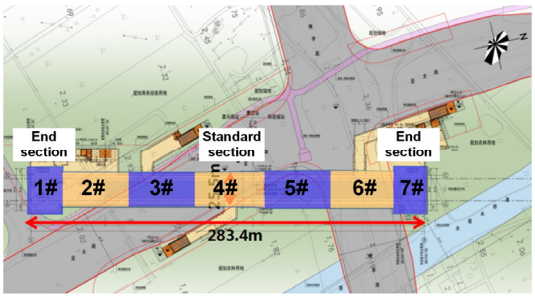

Figure 1. General layout of the Station.

During construction, the first-phase caissons (1#, 3#, 5#, and 7#) were sunk synchronously. Subsequently, the second-phase caissons (2#, 4#, and 6#) were installed simultaneously. Finally, the gaps between adjacent caissons were interconnected to form the integrated station structure.

3 NUMERICAL MODELLING

3.1 *Information of finite element model*

To investigate the environmental impact induced by sequential penetration of twin caissons and the structural influence of second-phase caisson on first-phase one, finite element analysis was conducted on two adjacent standard section caissons (first-phase 3# and second-phase 4#). Leveraging structural symmetry to reduce computational demands, a half-model was established as illustrated in Figure 2. Each caisson measures 44.42 m in length, 25.5 m in width, and 25 m in depth, with 1-m-thick sidewalls and 0.5-m-thick internal partitions. The soil domain extends 200 m longitudinally, 63 m transversely, and 50 m vertically.

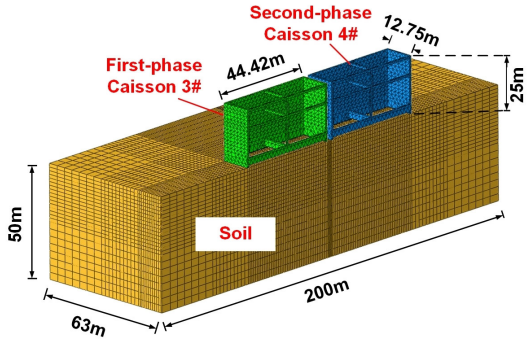

Figure 2. Schematic diagram of half finite element model.

Penalty-function-based contact was implemented between caissons and soil with a friction coefficient of 0.5, while the soil excavation process within caissons was simulated using the "Model change" technique. Given the adoption of undrained sinking in construction, effective unit weight was assigned to the soil to ensure simulation fidelity. Since Layer 4 (gray silty clay) constitutes over 50% of the penetration depth and its geomechanical properties are well-characterized, a homogeneous stratum representing this layer was modeled using the simplified kinematic hardening model with von Mises failure criterion available in the finite element software Abaqus. This model can effectively capture the nonlinear performance of soil under undrained conditions. Material parameters for caissons and soil are detailed in Table 1 and Table 2 respectively.

Table 1. Material parameters of caissons.

Parameter	Value	Unit
Young's modulus	30	GPa
Poisson's ratio	0.3	-

Table 2. Material parameters of gray silty clay of Layer 4.

Parameter	Value	Unit
Young's modulus	69502	kPa
Poisson's ratio	0.495	-
Unit weight	16.4	kN/m^3
Undrained shear strength	27	kPa
Yield stress at zero plastic strain	2.7	kPa
Kinematic hard parameter C1	16712	-
Gamma 1	325	-

3.2 *Verification through empirical formulas*

For single caisson installations, Xu et al. (2014) derived an exponential surface settlement distribution equation based on field monitoring data during construction:

$$\delta_v = \delta_{vm} e^{-4.3\frac{d}{H}} \quad (1)$$

Where, d denotes the horizontal distance from the caisson wall; H represents the height of the caisson; and δ_{vm} indicates the maximum surface settlement when the penetration depth of caisson is H.

Their study further established that maximum surface settlement δ_{vm} ranges between 0.063% and 1.360% of the penetration depth H, with a mean value of 0.715%.

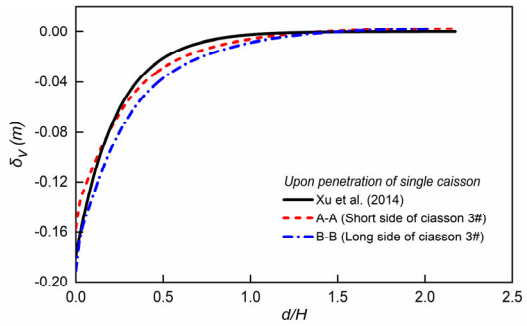

Figure 3. Verification of surface settlement due to caisson penetration.

Table 3. The normalized maximum surface settlement δ_{vm}/H.

Cross-section	δ_{vm}/H
A-A	0.628%
B-B	0.766%
Xu et al. (2014)	0.715%

To validate the finite element model proposed in Section 3.1, surface settlements were examined along two characteristic cross-sections (A-A and B-B in Figure 4) under the scenario of Caisson 3# penetrating to target depth. Figure 3 demonstrates remarkable consistency between the FEA results and empirical formulas in Xu et al. (2014), confirming the efficacy and precision of the numerical model. The analysis additionally revealed that surface settlements exhibit differential magnitudes along the long and short sides during penetration, with the maximum settlement occurring at the midpoint of the long side. Significant surface deformation is observed within a horizontal distance ratio of d/H = 0.55, beyond which caisson penetration exerts negligible influence on settlements.

Table 3 presents the normalized maximum surface settlement δ_{vm} at the midpoints of both the long and short sides of Caisson 3# relative to penetration depth H. The values are closely aligned with the mean value of 0.715% recommended by Xu et al. (2014).

4 COMPARISON OF INSTALLATION SCHEMES

In engineering practice, twin-caisson installation schemes can be categorized into two types based on execution sequence: synchronous installation and asynchronous installation. To identify the optimal scheme minimizing both ground settlement and structural response, this section employs numerical simulations to compare soil deformation patterns and structural responses of first-phase caisson under these installation methods. Model geometry and parameters remain identical to those established in Section 3. Five characteristic cross-sections shown in Figure 4 were selected for ground settlement analysis: Section A-A at the midpoint of the short side of Caisson 3#; Section B-B at the midpoint of the long side of Caisson 3#; Section C-C along the centerline axis of twin-caissons; Section D-D at the midpoint of the long side of Caisson 4#; Section E-E at the midpoint of the short side of Caisson 4#.

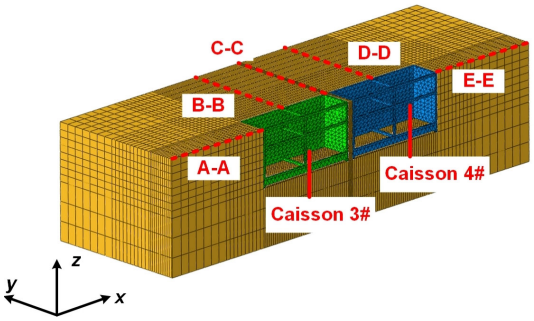

Figure 4. Three characteristic cross-sections diagram.

4.1 *Asynchronous installation*

Figure 5 presents the distribution of ground settlement with radial distance under the asynchronous installation scheme. The results demonstrate that when the second-phase Caisson 4# reached its target depth, the ground settlement at Section A-A of the first-phase Caisson 3# exhibits a slight increase (as shown in Figure 5(a)), while Section B-B shows a more pronounced increase (as shown in Figure 5(b)). This observation indicates that the installation of second-phase caissons has a relatively limited influence range on ground movement around first-phase caissons. Notably, Figure 5(c) shows that the induced ground settlement at Section C-C between the twin caissons is greater than that on either side, which can be attributed to the interaction effect between adjacent caissons.

Table 4 summarizes the maximum ground settlement values at each cross-section when both caissons reached their target depths. The data reveal that the maximum ground settlement in the asynchronous installation scheme occurs at the midpoint of the long side of the first-phase caisson. Furthermore, the ground settlement induced by the second-phase caisson installation is more significant than that caused by the first-phase caisson.

In addition to soil deformation, 0 presents the spatial displacement and rotational displacement components of the first-phase caisson when the second-phase caisson reached its target depth. The results clearly show that the first-phase caisson develops a tilting tendency toward the second-phase caisson, demonstrating the "mutual attraction effect" between twin caissons during installation.

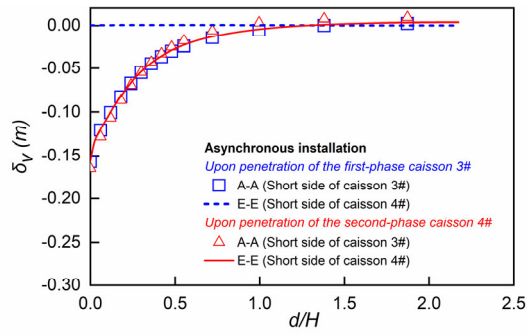

(a) Cross-section A-A and E-E

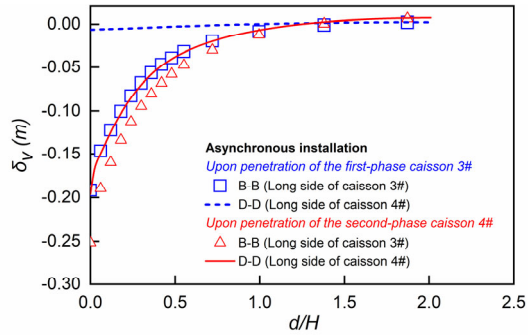

(b) Cross-section B-B and D-D

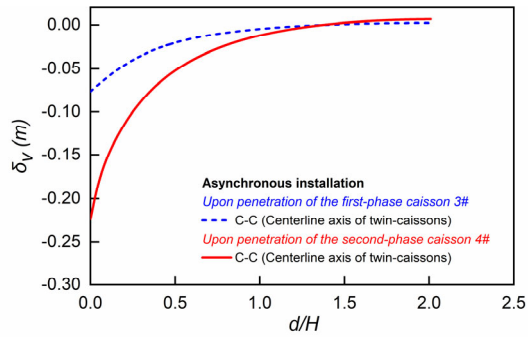

(c) Cross-section C-C

Figure 5. The distribution of ground settlement with radial distance under the asynchronous installation scheme.

Table 4. Maximum surface settlement of each cross-section under the asynchronous installation scheme.

Cross-section	Values *(m)*			
	First-	δ_{vm}/H	Second-	δ_{vm}/H
A-A	-0.1570	0.628%	-0.1650	0.660%
B-B	-0.1914	0.766%	-0.2514	1.006%
C-C	-0.0764	0.306%	-0.2238	0.895%
D-D	-0.0063	0.025%	-0.1960	0.784%
E-E	0.0003	0.001%	-0.1558	0.623%

Analysis in Section 3.2 reveals a parabolic settlement trough in the surrounding soil during caisson penetration. During sequential penetration of twin caissons, this soil movement pattern induced by the second-phase caisson acts upon the first-phase one, generating a downward dragging tendency on the first-phase caisson (as indicated by *U3* in 0) and a rotational tendency due to different far- and near-field effects (as indicated by *UR2* in 0). These mechanisms constitute a key origin of the "mutual attraction effect". Moreover, owing to this effect, the first-phase caisson undergoes certain passive displacements even after reaching its target depth, thereby imposing additional impacts on the surrounding environment. Consequently, under the combined influence of sequential caisson penetration and the mutual attraction effect, the maximum surface settlement in the asynchronous installation

scheme appears at the midpoint of the long side of the first-phase caisson.

Table 5. The spatial displacement and rotational displacement components of the first-phase caisson under the asynchronous installation scheme.

Components	Values
U1 (m)	-0.0132
U2 (m)	0
U3 (m)	-25.0814
UR1 (rad)	0
UR2 (rad)	0.0031
UR3 (rad)	0

Where, *U* is spatial displacement, and *UR* is rotational displacement, *UR2* represents rotation around the y-axis; 1、2、3 respectively represent the x、y、z directions in Figure 4.

4.2 *Synchronous installation*

Figure 6 presents the distribution of ground settlement with radial distance under the synchronous installation scheme. The results demonstrate that under the synchronous installation, due to structural symmetry, nearly identical final ground settlements occur at cross-sections A-A and E-E, as well as B-B and D-D. As shown in Figure 6(a), the influence of synchronous installation on soil movement adjacent to the caisson's short sides is negligible. However, it induces a slight increase in soil displacement along the caissons' long sides (as shown in Figure 6(b)). Furthermore, Figure 6(c) shows that interaction effects between synchronously installed twin caissons generate significantly larger vertical displacements in the soil between the caissons, similar to asynchronous installation.

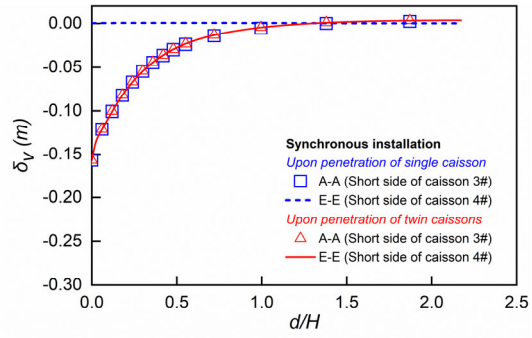

(a) Cross-section A-A and E-E

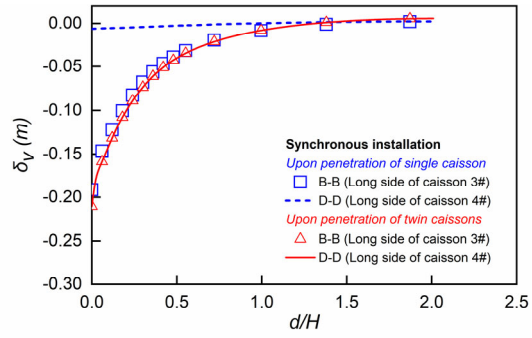

(b) Cross-section B-B and D-D

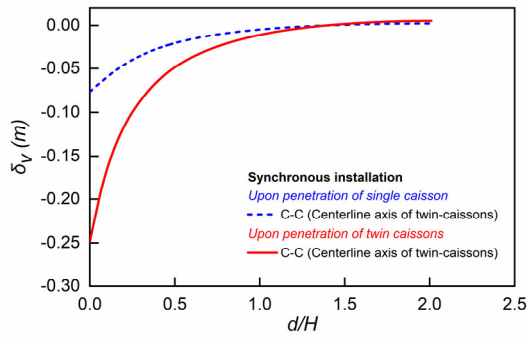

(c) Cross-section C-C

Figure 6. The distribution of ground settlement with radial distance under the synchronous installation scheme.

Table 6. Maximum surface settlement of each cross-section under the synchronous installation scheme.

Cross-section	Values *(m)*			
	Single	δ_{vm}/H	Twin	δ_{vm}/H
A-A	-0.1570	0.628%	-0.1580	0.632%
B-B	-0.1914	0.766%	-0.2105	0.842%
C-C	-0.0764	0.306%	-0.2483	0.993%
D-D	-0.0063	0.025%	-0.2105	0.842%
E-E	0.0003	0.001%	-0.1580	0.632%

Table 7. The spatial displacement and rotational displacement components of the first-phase caisson under the synchronous installation scheme.

Components	Values
U1 (m)	0.0012
U2 (m)	0
U3 (m)	-25
UR1 (rad)	0
UR2 (rad)	0.0018
UR3 (rad)	0

Table 6 also summarizes the maximum ground settlement values at each cross-section. The data shows that the maximum ground settlement in the synchronous installation scheme occurs at the midpoint of the twin caissons, which is different from the result of asynchronous installation.

Table 7 presents the spatial and rotational displacement components of Caisson 3# under the synchronous installation scheme. Due to structural symmetry, the displacement components of Caisson 4# exhibit an equal magnitude but opposite direction, forming a mirrored relationship.

Similar to the asynchronous installation scheme, under the synchronous installation scheme, the soil movement patterns induced by the penetration of both caissons act equally upon each other, resulting in a "mutual attraction effect" that draws the twin caissons closer (as indicated by *UR2* in Table 7). Due to the strong symmetry inherent in synchronous installation, the additional influence exerted by the passive displacements of each caisson on the surrounding soil exhibits corresponding symmetry. With the C–C section between the two caissons serving as the axis of symmetry, this region experiences the most significant superposition of effects, which explains why the maximum surface settlement in the synchronous installation scheme occurs at Section C–C.

4.3 *Discussion*

Analysis of maximum surface settlement across all cross-sections in Table 4 and Table 6 reveals that when both caissons reach their target depth, the maximum settlement at each section increases to varying degrees under either asynchronous or synchronous installation schemes.

Table 8 compares the results between asynchronous and synchronous installation schemes. The data of the synchronous

installation scheme demonstrate its superior effectiveness in minimizing soil disturbance around the caissons and reducing structural orientation changes. Consequently, synchronous installation can be regarded as the optimal scheme for twin-caisson installations to mitigate environmental impact.

Table 8. Comparison of the results of two installation schemes.

Schemes	Asynchronous	Synchronous
δ_{vm} *(m)*	-0.2514	-0.2483
U1 (m)	-0.0132	0.0012
UR2 (rad)	0.0031	0.0018

Moreover, due to inter-caisson interaction effect, soil deformation around twin caissons cannot be linearly superimposed using single-caisson results, but rather exhibits nonlinear superposition behavior. This study defines this phenomenon as the "mutual attraction effect", which, owing to its reproducible interaction mechanism, can be extended to multiple caissons or even caissons group. It should be noted that the manifestation of this effect varies with the penetration sequence, as reflected in both the location and magnitude of the maximum surface settlement. Furthermore, the presence of this effect increases the risk of caisson tilting during penetration, thereby endangering the safety of the project. In summary, the mutual attraction effect in multi-caisson penetration poses a significant challenge to field construction. It requires not only the selection of a suitable penetration sequence based on environmental impact considerations, but also the implementation of adequate corrective measures during penetration to prevent tilting and more serious consequences. The following sections of this study will conduct parametric studies, aiming to explore strategies for controlling the impact of the mutual attraction effect on the surrounding environment to the greatest extent possible.

5 PARAMETRIC STUDIES

The preceding analysis confirms that the synchronous installation scheme represents the optimal choice for mitigating surface settlement and structural response. Consequently, this scheme is adopted to investigate "mutual attraction effect" through a series of parametric studies. This section focuses on three dimensionless parameters: the normalized penetration depth (h_p/H), the normalized horizontal spacing between caissons (S_p/H) and the soil-caisson interface friction coefficient (α), with specific values detailed in Table 9. Subsequent sections present how variations in these parameters influence maximum surface settlement and structural response of Caisson 3#.

Table 9. Values of each dimensionless parameters.

Dimensionless parameters	Values
h_p/H	0.2, 0.4, 0.6, 0.8, 1.0
S_p/H	0.06, 0.10, 0.14, 0.18, 0.22
α	0.1, 0.2, 0.3, 0.4, 0.5

Where, h_p is the penetration depth, S_p is the horizontal spacing between caissons, H is the height of the caisson.

5.1 *Horizontal spacing between caissons*

Figure 7 illustrates the relationships between inter-caisson horizontal spacing and maximum surface settlement, spatial displacement, and rotational displacement at different penetration depths. As revealed in Figure 7(a), maximum surface settlement gradually decreases with increasing horizontal spacing. Notably, within a specific spacing range, the variation rates of maximum surface settlement across penetration depths remain similar. This phenomenon can be attributed to the dominance of penetration resistance – primarily governed by caisson wall friction and tip resistance – in controlling surface settlement, whereas horizontal spacing exhibits minimal influence on penetration resistance. Moreover, Figure 7(a) reveals that the normalized maximum surface settlements δ_{vm}/h_p relative to penetration depth h_p during twin-caisson penetration consistently exceed the mean value of 0.715% recommended by Xu et al. (2014).

As depicted in Figure 7(b) and (c), both horizontal and rotational displacements of the Caisson 3# progressively diminish with increased spacing. This implies that as horizontal spacing expands, the "mutual attraction effect" between twin caissons weaken to negligible level: maximum surface settlement approaches value observed during single-caisson penetration, while horizontal and rotational displacements converge toward zero.

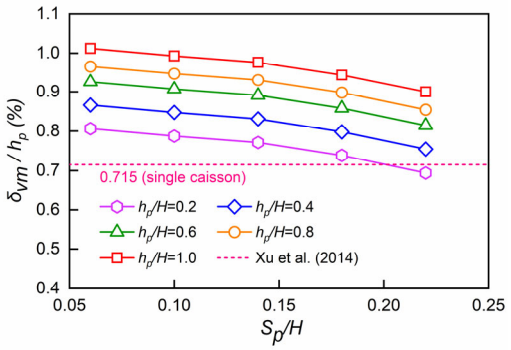

(a) Normalized maximum surface settlements.

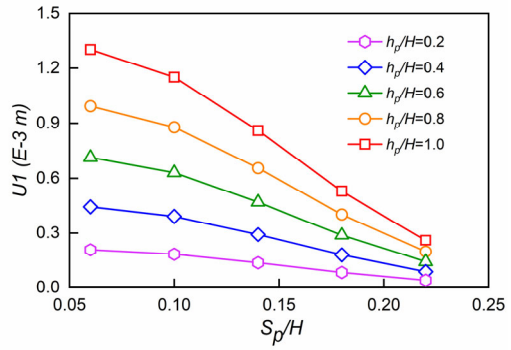

(b) Spatial displacement.

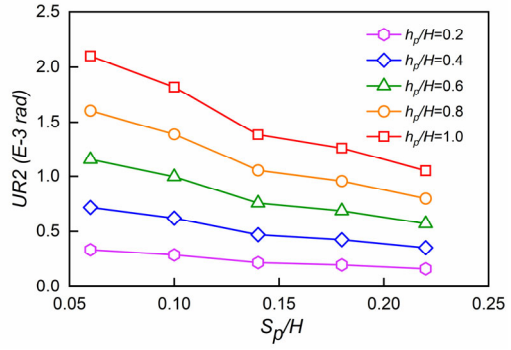

(c) Rotational displacement.

Figure 7. The influence of horizontal spacing between caissons at different penetration depths on δ_{vm}/h_p, *U1* and *UR2*.

5.2 *Friction coefficient*

Figure 8 illustrates the relationships between the soil-caisson interface friction coefficient and maximum surface settlement, spatial displacement, and rotational displacement at varying penetration depths. As evidenced in Figure 8(a), (b) and (c), δ_{vm}, *U1*, and *UR2* all exhibit nonlinear growth with increasing

interface friction coefficient. This trend arises because higher friction coefficient enhances contact strength between the caisson and soil, rendering surrounding soil more responsive to structural movements, thereby intensifying the "mutual attraction effect" of twin-caissons. Consequently, both soil and structural responses intensify, with this effect becoming increasingly pronounced at greater penetration depths.

Furthermore, the relationship between normalized maximum surface settlements δ_{vm}/h_p and recommended values by Xu et al. (2014), as demonstrated in Figure 8(a), provides additional validation for the friction coefficient value at 0.5 adopted in this study. It also indicates that empirical approaches for predicting maximum surface settlement necessitate reduction factors when interface friction coefficients decrease.

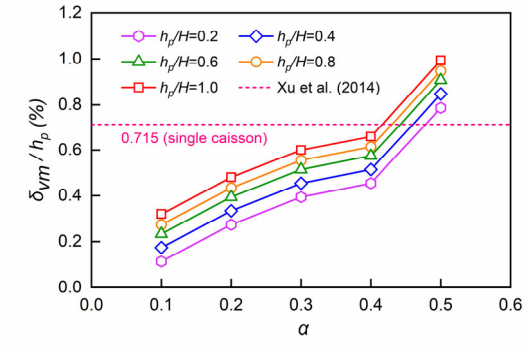

(a) Normalized maximum surface settlements.

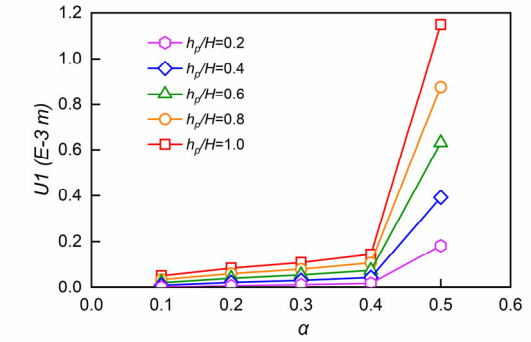

(b) Spatial displacement.

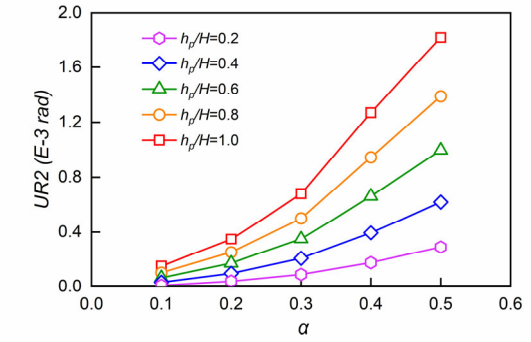

(c) Rotational displacement.

Figure 8. The influence of friction coefficient at different penetration depths on δ_{vm}/h_p, *U1* and *UR2*.

6 CONCLUSIONS

This study investigates the optimal installation sequence for twin-caisson penetration using finite element analysis, and examines environmental impact mechanisms and the "mutual attraction effect" of twin-caissons through parametric studies. The principal conclusions are summarized as follows:

1. Under both asynchronous and synchronous installation schemes, the "mutual attraction effect" occurs due to inter-caisson interaction. Soil deformation around twin caissons demonstrates nonlinear superposition behavior.
2. Comparative analysis confirms that synchronous installation generates minimal surface settlement and structural response, establishing it as the optimal scheme for twin-caisson installation.
3. In synchronous installation, increased inter-caisson spacing progressively diminishes the "mutual attraction effect" to negligible level. Maximum surface settlement converges toward single-caisson penetration value, while horizontal and rotational displacements converge to zero.
4. Elevated soil-caisson interface friction coefficient enhances contact strength, heightening soil sensitivity. This change will enhance the "mutual attraction effect" of twin-caissons, causing nonlinear growth trends in soil deformation, structural response of caisson itself.

These findings provide scientific basis for practical engineering design, enabling safer, more efficient, and less disruptive underground construction in sensitive urban environment.

7 ACKNOWLEDGEMENTS

This work was financially supported by the Natural Science Foundation of Shanghai (Grant No.23ZR1468500). This support is gratefully acknowledged.

8 REFERENCES

Huang, M.S., Li, H., Yu, J., Zhang, C.R., and Ni, Y.P. 2023. On the simplified method for evaluating tunnel response due to overlying foundation pit excavation. *Transportation Geotechnics* 42, 101048.

Lai, F.W., Zhang, N.N., Liu, S.Y., Sun, Y.X., and Li, Y.L. 2021. Ground movements induced by installation of twin large diameter deeply-buried caissons: 3D numerical modeling. *Acta Geotechnica* 16, 2933-2961.

Le, B.T., Goodey, R.J., and Divall, S. 2019. Subsurface ground movements due to circular shaft construction. *Soils and Foundations* 59(5), 1160-1171.

New, B.M. 2017. Settlements due to shaft construction. *Tunnels & tunnelling international*, 16-17.

New, B.M., Bowers, K.H. 1994. Ground movement model validation at the Heathrow Express trial tunnel. *Tunnelling '94*. Springer, Boston, MA.

Newman, T., and Wong, H.Y. 2011. Sinking a jacked caisson within the London Basin geological sequence for the Thames Water Ring Main extension. *Quarterly Journal of Engineering Geology and Hydrogeology* 44(2), 221-232.

Xu, P.F., Li, Y.L., and Xu, W. 2014. Field measurement and analysis of influence of jacked open caisson construction on environments. *Rock and Soil Mechanics* 35(04), 1084-1094.

Yu, J., Li, H., Huang, M.S., Li, Y.H., Tan, J.Q.W., and Guo, Y.C. 2022. Timoshenko-beam-based response of existing tunnel to single tunneling underneath and numerical verification of opening and dislocation. *Computers and geotechnics* 147(7), 104757.

Zhang, Z.G., Huang, M.S., and Wang, W.D. 2013. Evaluation of deformation response for adjacent tunnels due to soil unloading in excavation engineering. *Tunnelling and Underground Space Technology* 38, 244-253.

Zhao, Y.S., and Zhou, B. 2013. High pressure rotary jet grouting pile with undrained caisson combined construction technology on nearby yangtze river levee protection. *Advanced Materials Research* 718-720, 1938-1944.